

Article

# Improving the Structural Ordering and Particle-Size Homogeneity of Li-Rich Layered $\text{Li}_{1.2}\text{Ni}_{0.13}\text{Co}_{0.13}\text{Mn}_{0.54}\text{O}_2$ Cathode Materials through Microwave Irradiation Solid-State Synthesis

Jotti Karunawan <sup>1,2,3</sup>, Oktaviardi Bityasmawan Abdillah <sup>3,4</sup>, Octia Floweri <sup>3,5</sup>, Mahardika Prasetya Aji <sup>6</sup>, Sigit Puji Santosa <sup>7</sup>, Afriyanti Sumboja <sup>3,8</sup> and Ferry Iskandar <sup>2,3,4,7,\*</sup>

- <sup>1</sup> Doctoral Program of Nanoscience and Nanotechnology, Graduate School, Institut Teknologi Bandung, Jl. Ganesha 10, Bandung 40132, Indonesia
  - <sup>2</sup> Research Center of Nanoscience and Nanotechnology, Institut Teknologi Bandung, Jl. Ganesha 10, Bandung 40132, Indonesia
  - <sup>3</sup> Collaboration Research Center for Advanced Energy Materials, National Research and Innovation Agency–Institut Teknologi Bandung, Jl Ganesha 10, Bandung 40132, Indonesia
  - <sup>4</sup> Department of Physics, Faculty of Mathematics and Natural Sciences, Institut Teknologi Bandung, Jl Ganesha 10, Bandung 40132, Indonesia
  - <sup>5</sup> Research Center for Advanced Materials, National Research and Innovation Agency (BRIN), Komplek Puspiptek Serpong, South Tangerang 15314, Indonesia
  - <sup>6</sup> Department of Physics, Universitas Negeri Semarang, Jalan Raya Banaran, Semarang 5022, Indonesia
  - <sup>7</sup> National Centre for Sustainable Transportation Technology (NCSTT), Jl. Ganesha 10, Bandung 40132, Indonesia
  - <sup>8</sup> Material Science and Engineering Research Group, Faculty of Mechanical and Aerospace Engineering, Institut Teknologi Bandung, Jl. Ganesha 10, Bandung 40132, Indonesia
- \* Correspondence: ferry@fi.itb.ac.id



**Citation:** Karunawan, J.; Abdillah, O.B.; Floweri, O.; Aji, M.P.; Santosa, S.P.; Sumboja, A.; Iskandar, F. Improving the Structural Ordering and Particle-Size Homogeneity of Li-Rich Layered  $\text{Li}_{1.2}\text{Ni}_{0.13}\text{Co}_{0.13}\text{Mn}_{0.54}\text{O}_2$  Cathode Materials through Microwave Irradiation Solid-State Synthesis. *Batteries* **2023**, *9*, 31. <https://doi.org/10.3390/batteries9010031>

Academic Editor: Biao Li

Received: 1 December 2022

Revised: 27 December 2022

Accepted: 28 December 2022

Published: 31 December 2022



**Copyright:** © 2022 by the authors. Licensee MDPI, Basel, Switzerland. This article is an open access article distributed under the terms and conditions of the Creative Commons Attribution (CC BY) license (<https://creativecommons.org/licenses/by/4.0/>).

**Abstract:**  $\text{Li}_{1.2}\text{Ni}_{0.13}\text{Co}_{0.13}\text{Mn}_{0.54}\text{O}_2$  (LNCM) has been intensively investigated owing to its high capacity and large voltage window. However, despite its high performance, the synthesis of LNCM can be challenging as it usually contains structural disorders and particle-size inhomogeneities, especially via a solid-state method. This work introduces microwave irradiation treatment on the LNCM fabricated via a solid-state method. The as-treated LNCM has low structural disorders, as indicated by the smaller cation mixing, better hexagonal ordering, and higher  $c/a$  ratio compared to the non-treated LNCM. Furthermore, the particle-size homogeneities of as-treated LNCM improved, as characterized by scanning electron microscopy (SEM) and particle size analyzer (PSA) measurements. The improved structural ordering and particle-size homogeneity of the treated sample enhances the specific capacity, initial Coulombic efficiency, and rate capability of the cathode material. The LNCM sample with 20 min of microwave treatment exhibits an optimum performance, showing a large specific capacity (259.84 mAh/g), a high first-cycle Coulombic efficiency (81.45%), and good rate capability. It also showed a stable electrochemical performance with 80.57% capacity retention after 200 cycles (at a charge/discharge of 0.2C/0.5C), which is 13% higher than samples without microwave irradiation.

**Keywords:** cycling stability; facile microwave synthesis; high-capacity cathode; lithium-ion battery; low cation mixing

## 1. Introduction

The utilization of Li-ion batteries (LIBs) has changed from powering personal electronic gadgets to the rapidly expanding popularity of electric vehicles (EVs), which demands versatile and cost-effective LIBs with high energy density [1]. The energy density of LIBs is determined by the specific capacity of the battery as well as the working voltage,

both of which are heavily influenced by the cathode materials [2,3]. Among the various cathodes reported so far, a Li-rich Mn-based cathodes has shown tremendous potential as the next generation LIB following its high specific capacity and wide voltage windows [4].

The Li-rich Mn-based cathode is extensively represented in the literature by two equal formulas:  $x\text{Li}_2\text{MnO}_3 \cdot (1-x)\text{LiTMO}_2$  and  $\text{Li}_{(1+y)}\text{TM}_{(1-y)}\text{O}_2$  (TM=Ni, Co, Mn) [5,6]. LNCM is an abbreviation for the formula  $0.5\text{Li}_2\text{MnO}_3 \cdot 0.5\text{LiNi}_{1/3}\text{Co}_{1/3}\text{Mn}_{1/3}\text{O}_2$ , which is one of the stoichiometric compositions that belongs to the group of Li-rich Mn-based cathode materials. This composition has been intensively investigated for its large theoretical capacity (>200 mAh/g) and high working voltage (>3.7 V vs. Li/Li<sup>+</sup>) [7]. However, activation of the  $\text{Li}_2\text{MnO}_3$  phase at the first cycle produces  $\text{O}_2$  gas that leaves oxygen vacancies as the product of oxygen evolution, leading to irreversible capacity that results in a low Coulombic efficiency at the first cycle, the migration of transition metals, and inferior cycling stability [8,9].

Moreover, synthesizing high-performance LNCM is challenging as the product usually contains structural disorders (i.e., cation mixing, structural defects, and stacking faults), which will reduce the performance and long-term stability of the LNCM [10]. The poor structural disorders can be indicated by the high hexagonal ordering revealed from XRD results, which can be quantified by a high  $I_{(003)}/I_{(104)}$  ratio, a low  $(I_{(006)}+I_{(102)})/I_{(101)}$  ratio (i.e., R-factor), and a high  $c/a$  ratio [11–13]. Cation mixing is one of the most common structural disorders in the layered cathode (e.g., LNCM), which occurs due to a close Bohr radius of  $\text{Li}^+$  and  $\text{Ni}^{2+}$ , i.e., 0.76 Å and 0.69 Å, respectively.  $\text{Li}^+$  may occupy 3a sites of the transition metal layer, while  $\text{Ni}^{2+}$  may occupy 3b sites of the Li layer, hampering the reversible intercalation/deintercalation of Li ions [14]. Cation mixing also leads to local structural collapse and accelerates the phase transformation, which often results in voltage fading and unstable cycling performance [15].

The introduction of dopants [16,17], structural modification [18,19], and surface modification [20,21] have been reported to minimize structural disorders in LNCM. Furthermore, the type and concentration of the structural disorders are significantly influenced by the synthesis process, particularly the precursors' composition, synthesis method, and synthesis parameters [22]. Among the various methods used to obtain LNCM, the solid-state approach is regarded as a simpler method than the solution-based synthesis (i.e., coprecipitation and sol-gel), which often requires an inert  $\text{N}_2$  environment to prevent  $\text{Mn}^{2+}$  and  $\text{Co}^{2+}$  from forming high-valence hydroxides species [22]. In addition, hydrothermal and solvothermal synthesis of LNCM may need a relatively high temperature and high-pressure conditions, which is challenging for its scaled-up production [23].

Solid-state synthesis of LNCM has been reported in the literature [24–26]. Generally, it is started by mixing the precursors in the solid phase or the wet phase with additional dispersant, followed by two steps of heat treatment. Unfortunately, most LNCM compounds obtained by the solid-state method exhibited an agglomerated morphology with inhomogeneous particle distribution, leading to non-uniform reactions at the interface and the formation of a cathode electrolyte interface (CEI), which reduces the cycling stability of the battery [22].

Microwave irradiation is a potential method that can be employed to treat the as-synthesized cathode materials [27]. Although its mechanism is not yet fully understood, microwave irradiation is known to cause a positive impact on the electrochemical performance of the cathode. Microwave treatment was utilized by Zhao et al. and Miao et al. on Li-rich Mn-based cathode materials that were produced via co-precipitation and hydrothermal synthesis, respectively. It could suppress the cation mixing in the samples, as indicated by the higher  $I_{(003)}/I_{(104)}$  in XRD results [28,29]. In accordance with the previous reports, Shi et al. also utilized microwave treatment on a hydrothermally synthesized Li-rich Mn-based cathode. The obtained sample showed an improved homogeneity of secondary particles and enhanced structural ordering, as indicated by the lower cation mixing and a lower R-factor [30].

Inspired by previous results, we introduce microwave treatment on the LNCM obtained by a facile solid-state method, employing a ball-milling technique. This combination efficiently produces LNCM with a pure phase, a well-ordered crystal structure, low cation mixing, and good particle-size homogeneity. Apart from the physical properties of the LNCM, we also investigated the influence of microwave irradiation on the electrochemical performance of LNCM as a cathode material in LIBs. This study showed that microwave treatment improves the specific capacity, initial Coulombic efficiency, rate capability, and cycling stability of the LNCM prepared via a solid-state method. Furthermore, the positive effect of microwave irradiation on alleviating voltage fading and phase transformation in LNCM is also investigated and explained in this work.

## 2. Materials and Methods

### 2.1. Preparation of LNCM

The LNCM was prepared via an acetate precursor-based solid-state synthesis. A stoichiometric amount (1.2:0.13:0.13:0.54) of lithium acetate dihydrate ( $\text{Li}(\text{CH}_3\text{CO}_2)\cdot 2\text{H}_2\text{O}$ , 99.0%, Sigma Aldrich), nickel acetate tetrahydrate ( $\text{Ni}(\text{CH}_3\text{CO}_2)_2\cdot 4\text{H}_2\text{O}$ , 98.0%, Sigma Aldrich), cobalt acetate tetrahydrate ( $\text{Co}(\text{CH}_3\text{CO}_2)_2\cdot 4\text{H}_2\text{O}$ , 99.99%, Merck), and manganese acetate tetrahydrate ( $\text{Mn}(\text{CH}_3\text{CO}_2)_2\cdot 4\text{H}_2\text{O}$ , 99.0%, Merck) were weighed and dissolved in 100 ml of ethanol. The mixture was stirred for 30 min to obtain a homogeneous solution. The obtained solution was heated at 120 °C in a vacuum oven for 12 h until dry. The produced sample was crushed in a ball mill for 30 min and then heated for 4 h at 400 °C in a furnace. The calcined powder was subsequently treated with microwave irradiation using a Panasonic NN-ST34HM (800 watt) microwave oven. The microwave temperature was set to 185 °C, and the sample was treated for 0, 10, 20, and 30 min. All samples were then heated further at 850 °C for 6 h in ambient atmosphere at a heating rate of 5 °C/min.

### 2.2. Materials Characterizations

The thermal decomposition of the precursors was investigated by a thermogravimetric analyzer (TGA, Hitachi STA7300) within the range of 30 – 1000 °C at 10 °C/min under an atmosphere of air. An X-ray diffraction system (XRD, Bruker D8 Advance,  $\text{K}\alpha$  wavelength: 1.5406 Å) was used to characterize the crystal structure of the samples. The lattice parameter was determined by Rietveld refinement using Profex software [31]. The morphology of the sample was analyzed using scanning electron microscopy (SEM, Hitachi SU3500). Meanwhile, a particle size analyzer (PSA, Horiba SZ-100) was employed to measure the particle size of the samples, after 10 min of sonication of the solution containing 0.01 g of samples in the 15 ml of DI water.

### 2.3. Electrochemical Properties Characterizations

The cathodes were fabricated using the doctor blade technique. Slurries containing LNCM active materials, carbon black, and polyvinylidene difluoride (PVDF) binder (ratio 8:1:1) with N-methyl-2-pyrrolidone (NMP) as a solvent were prepared before casting them on aluminum foil. The process was followed by vacuum drying at 100 °C overnight to completely remove the solvent. The dried cathode sheet was punched into a disc with a diameter of 16 mm and assembled together with Li metal, Celgard 2400 separator, and organic electrolyte containing  $\text{LiPF}_6$  (1 M) dissolved in a mixture of EC:DEC:DMC (1:1:1). The assembly was performed in a glovebox that was filled with argon, and both the water and oxygen concentrations were kept at less than 0.1 ppm. Charge–discharge measurements were carried out at room temperature using a Neware BTS4000 battery tester along the voltage ranges of 2–4.8 V and 2–4.6 V. These measurements were carried out after several hours of resting period to stabilize the voltage response. Electrochemical impedance spectroscopy (EIS) and cyclic voltammetry (CV) measurements were conducted using a potentiostat galvanostat (Parstat 3000 A). EIS was performed over a frequency of 100 kHz – 0.1 Hz, while CV was scanned along a voltage window of 2 – 5 V (vs.  $\text{Li}/\text{Li}^+$ ) with 0.1, 0.2, 0.3, and 0.5 mV/s scan rates. In order to examine the Li-ion diffusion in

the samples, CV measurements were performed at a variety of scan rates. The diffusion coefficient of Li-ion for the sample prepared with and without microwave treatment was analyzed using the Randles–Sevcik Equation (1) [32].

$$I_p = 0.4463 \cdot n^{3/2} \cdot F^{3/2} \cdot C \cdot A \cdot R^{-1/2} \cdot T^{-1/2} \cdot \tilde{D}^{1/2} \cdot v^{1/2} \quad (1)$$

The Randles–Sevcik equation correlates the peak current ( $I_p$ , A) with the Faraday constant ( $F$ , C/mol), Li initial concentration ( $n$ , mol/cm<sup>3</sup>), electrode surface area ( $A$ , cm<sup>2</sup>), gas constant ( $R$ , J/mol K), temperature ( $T$ , K), lithium diffusion coefficient ( $\tilde{D}$ , cm<sup>2</sup>/s), and CV scan rate ( $v$ , V/s).

### 3. Results and Discussions

TGA was conducted on the precursor mixture to find out the optimum temperature of the first calcination step (Figure S1). Significant weight loss (~52.8%) within the temperature range of 300–400 °C corresponds to the decomposition of organic components (i.e., acetate) [33]. Therefore, 400 °C was selected as the temperature for the first calcination process, producing LNCM samples in their oxide form. The microwave treatment was conducted on the LNCM samples after the first calcination step. The microwave irradiation was varied for 0 (i.e., without microwave treatment), 10, 20, and 30 min to obtain the optimal parameters of the microwave treatment. After treatment, the samples undergo the second calcination step. As reported in our previous report, 850 °C was selected as the second calcination temperature to obtain the good crystallinity of layered-layered LNCM [34].

After completing the second calcination as the last step of the synthesis procedure, the crystallinity of the samples was then characterized by XRD (Figure 1). All samples show sharp XRD peaks that are unique to the Li-rich layered structure, consisting of peaks from the hexagonal  $\alpha$ -NaFeO<sub>2</sub> structure of layered LiTMO<sub>2</sub> (TM = Ni, Co, Mn) ( $R\bar{3}m$ ) and peaks from the monoclinic structure of layered Li<sub>2</sub>MnO<sub>3</sub> (space group  $C/2m$ ) [35]. No defect structure and impurity peak appear in the sample. Meanwhile, the obvious and distinct split of the (006)/(102) and (108)/(110) peaks across all samples suggests excellent layered structure ordering, indicating the successful formation of the layered-layered LNCM structure [36].

Rietveld refinement was then performed to further explore the influence of microwave treatment on the structure of the samples in more detail (Figure 2) and the refinement results are displayed in Table 1. The intensity ratio of (003) to (104) peaks ( $I_{(003)}/I_{(104)}$ ) for the layered structure is usually employed to determine the degree of cation mixing. It can be seen that the  $I_{(003)}/I_{(104)}$  value of all samples is higher than 1.2, indicating the low cation mixing of all LNCM samples [37]. Moreover, the LNCM sample with 20 min of microwave treatment shows the highest  $I_{(003)}/I_{(104)}$  value (i.e., 2.015), indicating the lowest Li<sup>+</sup>/Ni<sup>2+</sup> mixing degree among the samples. This value is higher than previously reported LNCM samples obtained via other synthesis methods (Supplementary Information Table S1), indicating that microwave treatment of LNCM synthesized by the solid-state method is a promising strategy to minimize structural disorders on the LNCM cathode materials.

Furthermore, the R-factor, which is defined as the value of  $(I_{(006)}+I_{(012)})/I_{(101)}$ , is widely used to gauge how good the hexagonal ordering is within the layered structure [38]. The R-factor of all samples is lower than 0.5, suggesting their well-ordered structure. Accordingly, the sample with 20 min of microwave treatment has the lowest R-factor, and, hence, possesses the best structural ordering among the samples. The low cation-mixing and high structural ordering of the microwave-irradiated sample indicates the positive effect of microwave treatment, as can be seen from the XRD patterns of the samples taken before and after microwave irradiation (Figure S2 and Table S2).

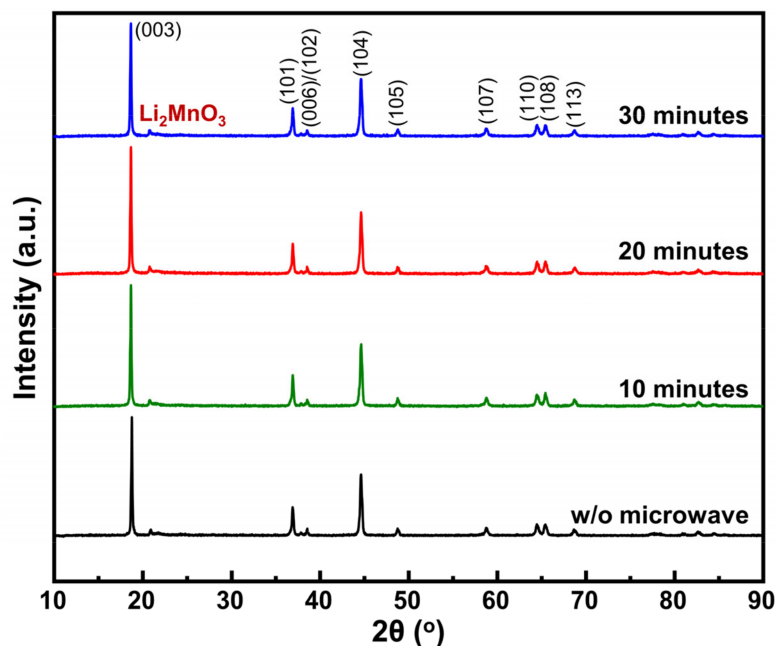


Figure 1. XRD patterns for LNCM with different microwave irradiation times: without microwave, 10 min, 20 min, and 30 min.

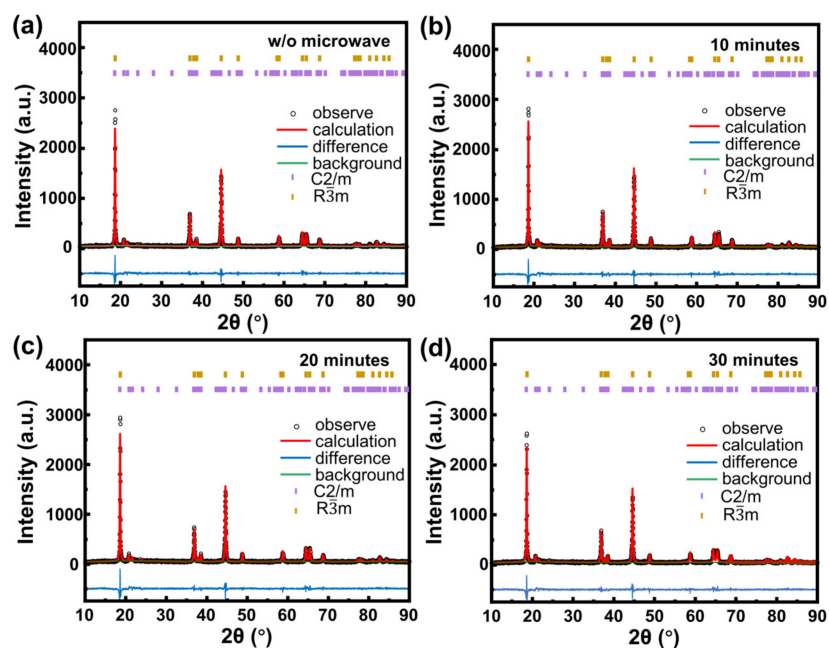


Figure 2. Rietveld refinement result of all LNCM samples prepared (a) without microwave irradiation (without microwave), and with (b) 10, (c) 20, and (d) 30 min of microwave irradiation.

Table 1. The refined lattice parameter of the LNCM samples.

Sample	$c$ (Å)	$a$ (Å)	$cla$	$I_{(003)}/I_{(104)}$	$(I_{(006)}+I_{(012)})/I_{(101)}$	$R_{wp}$ (%)
w/o microwave	14.2378	2.8513	4.9934	1.909	0.4431	13.16
10 min	14.2418	2.8515	4.9945	1.923	0.4154	12.74
20 min	14.2463	2.8521	4.9950	2.015	0.4011	12.98
30 min	14.2492	2.8532	4.9940	1.946	0.4326	13.03

The  $c$  and  $a$  lattice parameter represent the interslab distance and interlayer metal–metal distance, respectively. A high  $c/a$  ratio corresponds to facile Li-ion diffusion, which positively affects the rate capability of the battery [39]. Table 1 shows the increase in  $c/a$  ratio with the duration of microwave irradiation. The LNCM sample with 20 min of microwave treatment has the highest  $c/a$  ratio, indicating the optimal parameter for facile Li-ion diffusion. The significant increase in lattice parameter  $a$  after 30 min of irradiation caused the decrease in the  $c/a$  ratio in the sample, which probably corresponds to the high formation of reduced transition metals (i.e.,  $\text{Mn}^{3+}$ ) [40].

Furthermore, both  $c$  and  $a$  of the samples with microwave treatment are larger than those without microwave treatment, suggesting the structural expansion of the microwave-treated samples in both the  $c$  and  $a$  direction. The longer lattice parameter  $a$  can be associated with the reduction of the transition metal cation (e.g.,  $\text{Mn}^{4+} \rightarrow \text{Mn}^{3+}$ ) caused by the increase in cation radius of the transition metal [17,41]. On the other hand, the rise of the  $c$  lattice parameter can be attributed to the minor formation of oxygen vacancies during microwave irradiation [42].

The SEM images of all LNCM samples shown in Figure 3 demonstrate a uniform platelet shape, identical to the morphology of the cathode particles obtained by the solid-state method [24,34]. Meanwhile, the particle size distribution of each LNCM sample is represented by the bar diagrams in the inset of Figure 3. As microwave irradiation reduces the tendency of the primary particles to agglomerate, the samples with microwave treatment (i.e., 10, 20, and 30 min of irradiation) exhibit a more homogeneous particle size distribution than the non-treated sample. The LNCM sample with 20 min of microwave treatment shows the most homogeneous particle size distribution, as shown by the narrowest size distribution. The uniform particle size provides a more homogenous interface reaction during contact with the electrolyte, which minimizes cathode electrolyte interface (CEI) formation and subsequently enhances capacity retention [22].

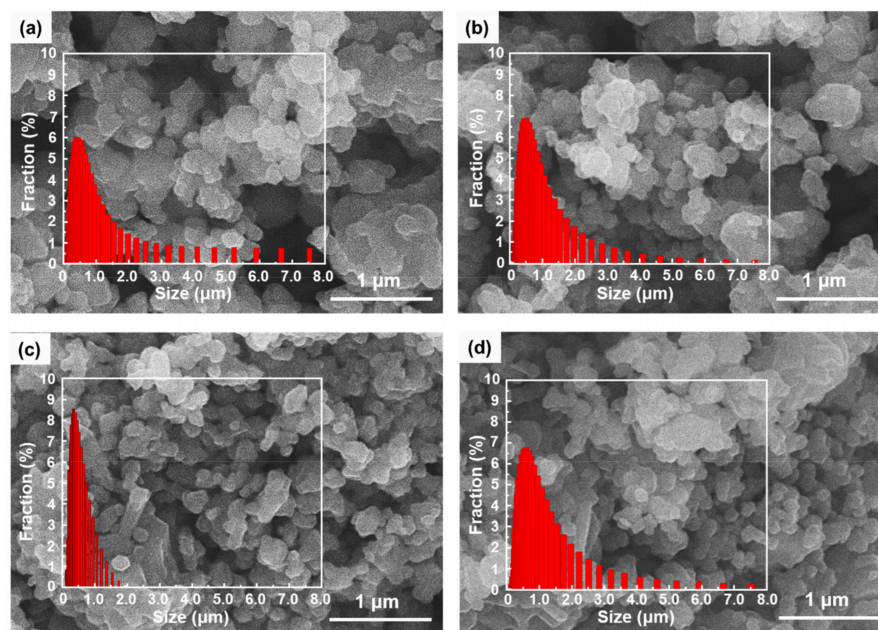


**Figure 3.** Morphology and particle size distribution of LNCM (a) without microwave irradiation, and with (b) 10, (c) 20, and (d) 30 min of microwave irradiation.

The charge–discharge measurement was used to characterize the electrochemical performance of LNCM samples. The voltage profile of all samples during the first cycle measured within the range of 2–4.8 V at a rate of 0.1 C (~20 mA/g) are given in Figure 4a. During the charging process, all samples exhibit two voltage plateaus. The smooth voltage incline below 4.5 V corresponds to cationic oxidation, while the long voltage plateau

above 4.5 V represents the activation of the  $\text{Li}_2\text{MnO}_3$  phase, which is responsible for providing the extra capacity [43]. The initial discharge capacities of LNCM samples without microwave irradiation and with microwave irradiation treatment for 10, 20, and 30 min are 232.92, 252.69, 259.84, and 243.77 mAh/g, respectively. The LNCM sample with 20 min of microwave treatment shows the largest specific capacity, which is in line with the XRD characterization that suggests the lowest structural disorders in the sample.

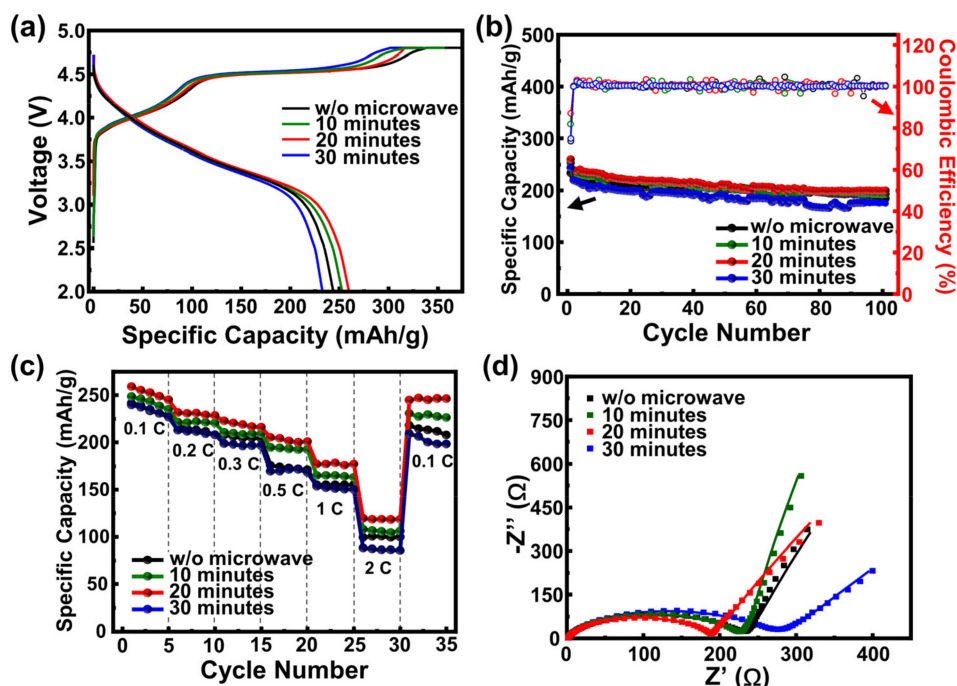


**Figure 4.** (a) Initial charge–discharge profile and (b) cycling stability of all LNCM samples, measured at a current density of 0.1 C (20 mA/g, 2–4.8 V) during the first activation cycle, followed by 100 cycles at 0.2 C (40 mA/g, 2–4.6 V); (c) rate capability of all LNCM samples, measured at various current densities within the 2–4.8 V voltage window; and (d) Nyquist plots of all LNCM samples.

Moreover, the initial Coulombic efficiency (ICE) of the LNCM without microwave irradiation is only 69.60%, while the ICE of samples with 10, 20, and 30 min of microwave irradiation are 74.58, 81.45, and 71.69%, respectively. The increasing ICE with the irradiation time corresponds to the low irreversible reaction upon the initial charge–discharge cycle. The sample with 20 min of microwave treatment shows the highest ICE, reflecting its good structural ordering and uniform particle size distribution, which resulted in the minimum generation of oxygen vacancies and  $\text{O}_2$  gas during  $\text{Li}_2\text{MnO}_3$  phase activation and small Li consumption during CEI formation [44].

The cycling stability of various LNCM samples is demonstrated in Figure 4b. After phase activation of  $\text{Li}_2\text{MnO}_3$  at the first cycle, the LNCM samples were tested for 100 cycles at 0.2 C (40 mA/g) with the voltage window of 2–4.6 V at room temperature. Samples with 0, 10, 20, and 30 min of microwave treatment showed a capacity retention of 76.19, 78.87, 81.22, and 71.60%, respectively. The results show optimum capacity retention at 20 min of irradiation time, which can be correlated with its lowest R-factor and most uniform particle size distribution among the samples, inducing a homogeneous reaction at the interface and minimum CEI formation [22,45].

The rate capability tests of LNCM samples were conducted under varied current densities (0.1 C–2 C) along the voltage range of 2–4.8 V (Figure 4c). Similar to the cycling stability test result, the sample with 20 min of microwave treatment shows the optimum rate capability, which can be related to the high  $c/a$  ratio of this sample. A high  $c/a$  ratio

enlarges the layer spacing, facilitating a facile Li ion diffusion and providing a large capacity at the high current density [46].

Each Nyquist plot of the samples obtained from EIS characterization displays a semi-circle located at the high to medium frequency domain and a straight profile at the lower frequency domain (Figure 4d). Figure S3 portrays the equivalent circuit that fitted the Nyquist plots, while Table S3 shows the fitting results. All samples possessed similar cell ohmic resistance ( $R_s$ ), indicating the similar resistance of the electrolyte and current collector [47].

Meanwhile, charge transfer resistance ( $R_{ct}$ ) of the LNCM sample is represented by the diameter of the semicircle. The sample with 20 min of microwave treatment has the smallest  $R_{ct}$ , suggesting its facile electrochemical reaction. Hence, according to material and electrochemical characterizations, the sample with 20 min of microwave treatment exhibits optimum performance, as indicated by the lowest cation mixing, the highest  $c/a$  ratio, the most homogeneous particle size distribution, and the superior electrochemical performance (i.e., large specific capacity, high initial Coulombic efficiency, superior rate capability, and stable cycling behavior).

To further investigate the impact of microwave irradiation on the LNCM synthesized via the solid-state method, cyclic voltammetry (CV) tests on the sample prepared without microwave irradiation and the sample prepared with 20 min of microwave treatment were conducted. First-cycle voltammograms of both samples measured with a 0.1 mV/s scan rate along the voltage window of 2–5 V show similar profiles, demonstrating their similar electrochemical characteristics (Figure 5a,b). The first peak at ~4.2 V during the anodic scan corresponds to transition metal oxidation (i.e.,  $Ni^{2+} \rightarrow Ni^{4+}$  and  $Co^{3+} \rightarrow Co^{4+}$ ). Meanwhile the second peak at ~4.7 V is correlated with the anionic redox reaction (i.e.,  $O^{2-} \rightarrow O^{n-}$  or  $O^{2-} \rightarrow O^-$ ), which happens during the activation of the  $Li_2MnO_3$  phase [48].

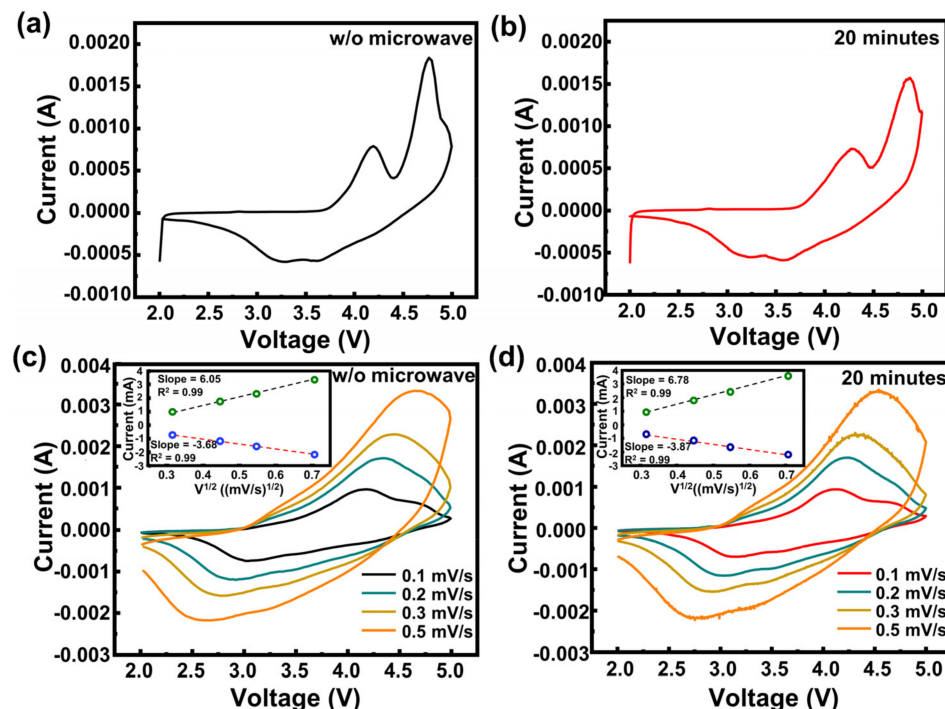


**Figure 5.** First-cycle cyclic voltammogram of LNCM samples (a) without microwave treatment and (b) with 20 min of microwave treatment. Cyclic voltammograms of LNCM samples (c) without microwave treatment and (d) with 20 min of microwave treatment measured at different scan rates (the inset shows the relationship between the peak current ( $I_p$ ) and the square of the scan rate ( $v^{1/2}$ )).

By comparing the second peak to the first peak ( $I(4.7\text{ V})/I(4.2\text{ V})$ ), the structural stability during the cycling test can be investigated. The sample without microwave

treatment and the sample with 20 min of microwave treatment revealed  $I(4.7\text{ V})/I(4.2\text{ V})$  values of around 2.325 and 2.239, respectively. The lower  $I(4.7\text{ V})/I(4.2\text{ V})$  value of the sample prepared with 20 min of microwave treatment indicates its more stable structure with a lower chance of oxygen loss [49]. The small oxygen loss alleviates the occurrence of irreversible process, especially during the initial charge–discharge cycle, which is consistent with the high ICE of the sample.

Figure 5c,d shows the voltammograms of both samples measured at various scan rates starting from 0.1 to 0.5 mV/s). The peak current observed at different scan rates can be related to the rate of the Li-ion intercalation and deintercalation process, in which the diffusion coefficient can be extracted from the Randles–Sevcik equation. In this work, the exact value of the diffusion coefficient ( $\tilde{D}$ ) was not calculated as some parameters are difficult to determine [50–52]. However, given that most of the parameters are constant, the slope of the linear relation between the peak current ( $I_p$ ) and the square of the scan rate ( $v^{1/2}$ ) can be directly related to the Li-ion diffusion coefficient. During the oxidation and reduction process, the slope value of  $I_p$  vs.  $v^{1/2}$  of 20 min sample is higher than that without microwave irradiation, indicating its higher diffusion coefficient as compared to the sample without microwave treatment. These results imply more efficient Li ion diffusion in the sample with 20 min of microwave treatment, leading to a better rate capability of this sample.

Figure 6a depicts the results of long-term cycling tests conducted on samples prepared with and without 20 min of microwave irradiation in order to determine the effect of microwave irradiation on the prevention of voltage fading. After conducting the first cycle at 0.1 C and a voltage window of 2–4.8 V as the activation step of the  $\text{Li}_2\text{MnO}_3$  phase, the cycling performance was tested within 2–4.6 V at 0.2 C and 0.5 C for charging and discharging, respectively. After 200 cycles, the cycling stability performance of the sample prepared with 20 min of microwave treatment shows higher capacity retention (80.57%) than the sample without microwave irradiation (66.78%), which is consistent with the results presented in Figure 4b for the cycling stability test. This capacity retention is in the higher range compared to the microwave treated LNCM sample obtained from solution-based synthesis (e.g., hydrothermal, co-precipitation), suggesting that microwave treatment of LNCM obtained by the solid-state method is a promising strategy to produce structurally stable LNCM (Supplementary Information, Table S4).

Figure 6b,c shows the selected normalized discharge capacity curves of different cycle numbers. The working voltage of both samples decreases with the number of cycles. This phenomenon is known as voltage fading, which is usually caused by the phase transformation from a layered to spinel structure [53]. The sample with 20 min of microwave irradiation shows a lower voltage fading than the sample without microwave irradiation, which may be correlated to the minimum phase transformation from the layered to spinel structure in this sample [54]. At the first cycle, oxygen evolution generates oxygen vacancies, allowing transition metal migration to Li sites, and eventually driving the formation of the spinel phase [53,55]. Microwave irradiation treatment can minimize oxygen loss, as indicated by the low  $I(4.7\text{ V})/I(4.2\text{ V})$  value observed at the first cycle during the CV scan. Therefore, the phase transformation of the sample with microwave irradiation during the long-term cycling is minimal compared to that without microwave irradiation. The minimum oxygen loss of the 20-minute-treated sample maintains the minimum change on the oxidation state of the cations during cycling, minimizing voltage decay [56]. Hence, the microwave treatment not only elevates the specific capacity, enhances initial Coulombic efficiency, and improves capacity retention and rate capability, but also suppresses the phase transformation and voltage fading in LNCM cathode materials.

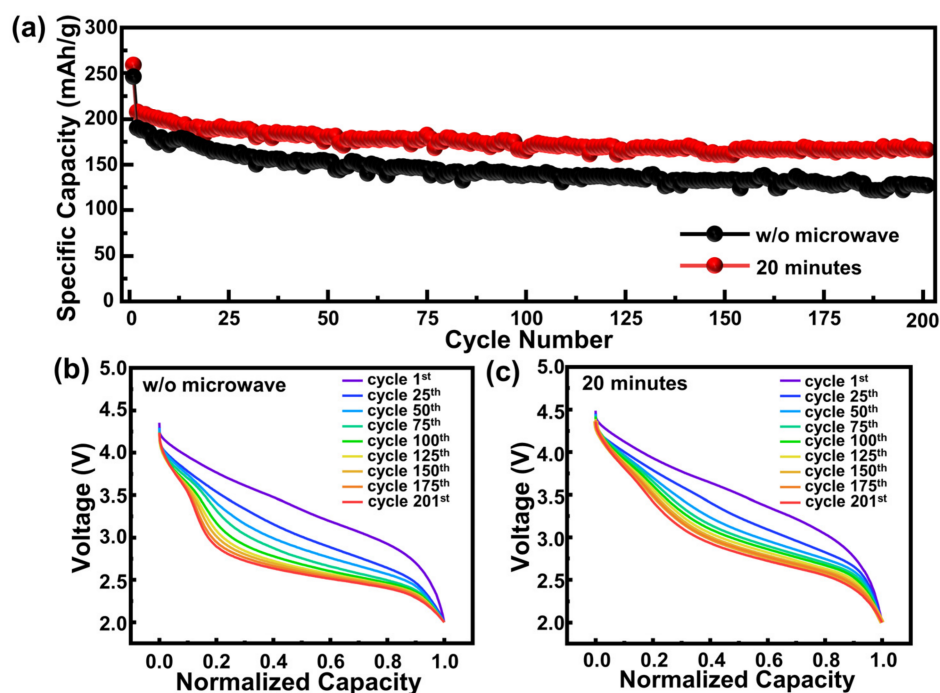


**Figure 6.** (a) Long-term cycling stability test of LNCM samples without and with 20 min of microwave treatment, and selected voltage discharge profiles of LNCM samples (b) without microwave treatment and (c) with 20 min of microwave treatment.

#### 4. Conclusions

In summary, LNCM cathode materials have been effectively synthesized through the use of a microwave-assisted solid-state technique. The experimental results indicate that microwave irradiation effectively improves the structural ordering and particle-size homogeneity of LNCM, and, hence, its electrochemical performance. By comparing the treatment period, 20 min of microwave irradiation on the LNCM is the optimal treatment time as indicated by its optimum initial Coulombic efficiency, specific capacity, capacity retention, and rate capability, which can be attributed to its minimum structural disorders and homogeneous particle size distribution. Moreover, microwave irradiation produces LNCM with a more stable structure, as indicated by the lower possibility of oxygen loss and voltage fading. These results suggest that microwave irradiation treatment on layered cathode materials is a facile treatment that can effectively mitigate structural disorders in the materials.

**Supplementary Materials:** The following supporting information can be downloaded at: <https://www.mdpi.com/article/10.3390/batteries9010031/s1>, Figure S1: TG curves of the precursor of the LNCM sample; Figure S2: XRD patterns of the LNCM sample after the first calcination step: (a) before microwave treatment and (b) after microwave treatment for 20 min; Figure S3: Basic equivalent circuit of the EIS measurement; Table S1: Comparison of the structural ordering with other works; Table S2: Full width at half maximum (FWHM) of the typical XRD peak of the LNCM sample after the first calcination step, before and after microwave treatment for 20 min; Table S3: Electrochemical impedance spectroscopy (EIS) fitting results of the LNCM cathode; Table S4: Comparison of the electrochemical performance with other works. (“References [28–30,57–65] are cited in the Supplementary Materials).

**Author Contributions:** Conceptualization, J.K., A.S. and F.I.; methodology, J.K., O.B.A., O.F., A.S. and F.I.; validation, M.P.A., S.P.S., A.S. and F.I.; formal analysis, J.K., O.B.A., O.F., A.S. and F.I.; investigation, J.K., O.B.A., O.F., A.S. and F.I.; resources, S.P.S. and F.I.; data curation, J.K.; writing—original draft preparation, J.K.; writing—review and editing, O.F., M.P.A., S.P.S., A.S. and F.I.; visualization, J.K. and O.B.A.; supervision, A.S. and F.I.; project administration, J.K., A.S. and F.I.; funding acquisition, A.S. All authors have read and agreed to the published version of the manuscript.

**Funding:** This work was funded by the Indonesian Endowment Fund for Education (LPDP) under the Southeast Asia-Europe Joint Funding Scheme for Research and Innovation.

**Data Availability Statement:** Not applicable.

**Conflicts of Interest:** The authors declare no conflict of interest.

## References

1. Ahmad, F.; Khalid, M.; Ketan, B. Development in Energy Storage System for Electric Transportation: A Comprehensive Review. *J. Energy Storage* **2021**, *43*, 103153. [[CrossRef](#)]
2. Eglitis, R.I.; Borstel, G. Towards a Practical Rechargeable 5 V Li Ion Battery. *Phys. Status Solidi Appl. Mater. Sci.* **2005**, *202*, 13–15. [[CrossRef](#)]
3. Eglitis, R.I. Theoretical Prediction of the 5 V Rechargeable Li Ion Battery Using  $\text{Li}_2\text{CoMn}_3\text{O}_8$  as a Cathode. *Phys. Scr.* **2015**, *90*, 94012. [[CrossRef](#)]
4. Ji, X.; Xia, Q.; Xu, Y.; Feng, H.; Wang, P.; Tan, Q. A Review on Progress of Lithium-Rich Manganese-Based Cathodes for Lithium Ion Batteries. *J. Power Sources* **2021**, *487*, 229362. [[CrossRef](#)]
5. Zuo, W.; Luo, M.; Liu, X.; Wu, J.; Liu, H.; Li, J.; Winter, M.; Fu, R.; Yang, W.; Yang, Y. Li-Rich Cathodes for Rechargeable Li-Based Batteries: Reaction Mechanisms and Advanced Characterization Techniques. *Energy Environ. Sci.* **2020**, *13*, 4450–4497. [[CrossRef](#)]
6. Zheng, J.; Myeong, S.; Cho, W.; Yan, P.; Xiao, J.; Wang, C.; Cho, J.; Zhang, J.G. Li- and Mn-Rich Cathode Materials: Challenges to Commercialization. *Adv. Energy Mater.* **2017**, *7*, 1601284. [[CrossRef](#)]
7. Zheng, H.; Han, X.; Guo, W.; Lin, L.; Xie, Q.; Liu, P.; He, W.; Wang, L.; Peng, D.L. Recent Developments and Challenges of Li-Rich Mn-Based Cathode Materials for High-Energy Lithium-Ion Batteries. *Mater. Today Energy* **2020**, *18*, 100518. [[CrossRef](#)]
8. Koga, H.; Croguennec, L.; Ménétrier, M.; Mannesiez, P.; Weill, F.; Delmas, C. Different Oxygen Redox Participation for Bulk and Surface: A Possible Global Explanation for the Cycling Mechanism of  $\text{Li}_{1.20}\text{Mn}_{0.54}\text{Co}_{0.13}\text{Ni}_{0.13}\text{O}_2$ . *J. Power Sources* **2013**, *236*, 250–258. [[CrossRef](#)]
9. Zhao, T.; Zhou, N.; Zhang, X.; Xue, Q.; Wang, Y.; Yang, M.; Li, L.; Chen, R. Structure Evolution from Layered to Spinel during Synthetic Control and Cycling Process of Fe-Containing Li-Rich Cathode Materials for Lithium-Ion Batteries. *ACS Omega* **2017**, *2*, 5601–5610. [[CrossRef](#)]
10. Wei, W.; Chen, L.; Pan, A.; Ivey, D.G. Roles of Surface Structure and Chemistry on Electrochemical Processes In Lithium-Rich Layered Oxide Cathodes. *Nano Energy* **2016**, *30*, 580–602. [[CrossRef](#)]
11. Chen, Z.; Meng, J.; Wang, Y.; Ma, Q.; Lai, F.; Li, Z.; Zhang, Q.; Li, D.; Zhong, S. Local Structure Modulation via Cation Compositional Regulation for Durable Li-Rich Layered Cathode Materials. *Electrochim. Acta* **2021**, *378*, 138138. [[CrossRef](#)]
12. Zhang, X.; Jiang, W.J.; Mauger, A.; Qilu; Gendron, F.; Julien, C.M. Minimization of the Cation Mixing in  $\text{Li}_{1+x}(\text{NMC})_{1-x}\text{O}_2$  as Cathode Material. *J. Power Sources* **2010**, *195*, 1292–1301. [[CrossRef](#)]
13. Yan, W.; Xie, Y.; Jiang, J.; Sun, D.; Ma, X.; Lan, Z.; Jin, Y. Enhanced Rate Performance of Al-Doped Li-Rich Layered Cathode Material via Nucleation and Post-Solvothermal Method. *ACS Sustain. Chem. Eng.* **2018**, *6*, 4625–4632. [[CrossRef](#)]
14. Sun, G.; Yin, X.; Yang, W.; Song, A.; Jia, C.; Yang, W.; Du, Q.; Ma, Z.; Shao, G. The Effect of Cation Mixing Controlled by Thermal Treatment Duration on the Electrochemical Stability of Lithium Transition-Metal Oxides. *Phys. Chem. Chem. Phys.* **2017**, *19*, 29886–29894. [[CrossRef](#)]
15. Cui, S.L.; Gao, M.Y.; Li, G.R.; Gao, X.P. Insights into Li-Rich Mn-Based Cathode Materials with High Capacity: From Dimension to Lattice to Atom. *Adv. Energy Mater.* **2022**, *12*, 2003885. [[CrossRef](#)]
16. Liu, S.; Liu, Z.; Shen, X.; Li, W.; Gao, Y.; Banis, M.N.; Li, M.; Chen, K.; Zhu, L.; Yu, R.; et al. Surface Doping to Enhance Structural Integrity and Performance of Li-Rich Layered Oxide. *Adv. Energy Mater.* **2018**, *8*, 1802105. [[CrossRef](#)]
17. Yang, J.; Chen, Y.; Li, Y.; Xi, X.; Zheng, J.; Zhu, Y.; Xiong, Y.; Liu, S. Encouraging Voltage Stability upon Long Cycling of Li-Rich Mn-Based Cathode Materials by Ta-Mo Dual Doping. *ACS Appl. Mater. Interfaces* **2021**, *13*, 25981–25992. [[CrossRef](#)]
18. Kim, S.; Cho, W.; Zhang, X.; Oshima, Y.; Choi, J.W. A Stable Lithium-Rich Surface Structure for Lithium-Rich Layered Cathode Materials. *Nat. Commun.* **2016**, *7*, 13598. [[CrossRef](#)]
19. Chen, M.; Liu, Y.; Zhang, Y.; Xing, G.; Tang, Y. Lithium-Rich Sulfide/Selenide Cathodes for next-Generation Lithium-Ion Batteries: Challenges and Perspectives. *Chem. Commun.* **2022**, *58*, 3591–3600. [[CrossRef](#)]
20. Lin, T.; Schulli, T.U.; Hu, Y.; Zhu, X.; Gu, Q.; Luo, B.; Cowie, B.; Wang, L. Faster Activation and Slower Capacity/Voltage Fading: A Bifunctional Urea Treatment on Lithium-Rich Cathode Materials. *Adv. Funct. Mater.* **2020**, *30*, 1909192. [[CrossRef](#)]
21. Karunawan, J.; Irham, M.A.; Widyardharma, P.H.; Floweri, O.; Aimon, A.H.; Iskandar, F. Effect of  $\text{NaTi}_2(\text{PO}_4)_3$  Coating on Improving Capacity Retention of Li-Rich. In Proceedings of the 2019 6th International Conference on Electric Vehicular Technology (ICEVT), Bali, Indonesia, 18–21 November 2019; pp. 11–13. [[CrossRef](#)]
22. Pimenta, V.; Sathiya, M.; Batuk, D.; Abakumov, A.M.; Giaume, D.; Cassaignon, S.; Larcher, D.; Tarascon, J.M. Synthesis of Li-Rich NMC: A Comprehensive Study. *Chem. Mater.* **2017**, *29*, 9923–9936. [[CrossRef](#)]
23. Liu, Q.; Hu, Z.; Chen, M.; Zou, C.; Jin, H.; Wang, S.; Chou, S.L.; Liu, Y.; Dou, S.X. The Cathode Choice for Commercialization of Sodium-Ion Batteries: Layered Transition Metal Oxides versus Prussian Blue Analogs. *Adv. Funct. Mater.* **2020**, *30*, 1909530. [[CrossRef](#)]

24. Zhou, L.Z.; Xu, Q.J.; Liu, M.S.; Jin, X. Novel Solid-State Preparation and Electrochemical Properties of  $\text{Li}_{1.13}[\text{Ni}_{0.2}\text{Co}_{0.2}\text{Mn}_{0.47}]\text{O}_2$  with a High Capacity by Acetate Precursor for Li-ion Batteries. *Solid State Ion.* **2013**, *249–250*, 134–138. [[CrossRef](#)]
25. Hao, W.; Zhan, H.; Chen, H.; Wang, Y.; Tan, Q.; Su, F. Solid-State Synthesis of  $\text{Li}[\text{Li}_{0.2}\text{Mn}_{0.56}\text{Ni}_{0.16}\text{Co}_{0.08}]\text{O}_2$  Cathode Materials for Lithium-Ion Batteries. *Particuology* **2014**, *15*, 18–26. [[CrossRef](#)]
26. Du, C.Q.; Zhang, F.; Ma, C.X.; Wu, J.W.; Tang, Z.Y.; Zhang, X.H.; Qu, D. Synthesis and Electrochemical Properties of  $\text{Li}_{1.2}\text{Mn}_{0.54}\text{Ni}_{0.13}\text{Co}_{0.13}\text{O}_2$  Cathode Material for Lithium-Ion Battery. *Ionics* **2016**, *22*, 209–218. [[CrossRef](#)]
27. Haruna, A.B.; Ozoemena, K.I. Effects of Microwave Irradiation on the Electrochemical Performance of Manganese-Based Cathode Materials for Lithium-Ion Batteries. *Curr. Opin. Electrochem.* **2019**, *18*, 16–23. [[CrossRef](#)]
28. Zhao, R.; Chen, Z.; Zhang, Y.; Du, P.; Chen, H. Ultrasonic/Microwave-Assisted Co-Precipitation Method in the Synthesis of  $\text{Li}_{1.1}\text{Mn}_{0.433}\text{Ni}_{0.233}\text{Co}_{0.233}\text{O}_2$  Cathode Material for Lithium-Ion Batteries. *Mater. Lett.* **2014**, *136*, 160–163. [[CrossRef](#)]
29. Miao, X.; Yan, Y.; Wang, C.; Cui, L.; Fang, J.; Yang, G. Optimal Microwave-Assisted Hydrothermal Synthesis of Nanosized  $x\text{Li}_2\text{MnO}_3 \cdot (1-x)\text{LiNi}_{1/3}\text{Co}_{1/3}\text{Mn}_{1/3}\text{O}_2$  Cathode Materials for Lithium Ion Battery. *J. Power Sources* **2014**, *247*, 219–227. [[CrossRef](#)]
30. Shi, S.; Wang, T.; Cao, M.; Wang, J.; Zhao, M.; Yang, G. Rapid Self-Assembly Spherical  $\text{Li}_{1.2}\text{Mn}_{0.56}\text{Ni}_{0.16}\text{Co}_{0.08}\text{O}_2$  with Improved Performances by Microwave Hydrothermal Method as Cathode for Lithium-Ion Batteries. *ACS Appl. Mater. Interfaces* **2016**, *8*, 11476–11487. [[CrossRef](#)]
31. Doebelin, N.; Kleeberg, R. Profex: A Graphical User Interface for the Rietveld Refinement Program BGMN. *J. Appl. Crystallogr.* **2015**, *48*, 1573–1580. [[CrossRef](#)]
32. Redel, K.; Kulka, A.; Plewa, A.; Molenda, J. High-Performance Li-Rich Layered Transition Metal Oxide Cathode Materials for Li-Ion Batteries. *J. Electrochem. Soc.* **2019**, *166*, A5333–A5342. [[CrossRef](#)]
33. Lv, C.; Peng, Y.; Yang, J.; Duan, X.; Ma, J.; Wang, T. Electrospun Nb-Doped  $\text{LiNi}_{0.4}\text{Co}_{0.2}\text{Mn}_{0.4}\text{O}_2$  Nanobelts for Lithium-Ion Batteries. *Inorg. Chem. Front.* **2018**, *5*, 1126–1132. [[CrossRef](#)]
34. Karunawan, J.; Floweri, O.; Santosa, S.P.; Sumboja, A.; Iskandar, F. Stable Layered-Layered-Spinel Structure of the  $\text{Li}_{1.2}\text{Ni}_{0.13}\text{Co}_{0.13}\text{Mn}_{0.54}\text{O}_2$  Cathode Synthesized by Ball-Milling Assisted Solid-State Method. *J. Electroanal. Chem.* **2022**, *907*, 116050. [[CrossRef](#)]
35. Thackeray, M.M.; Croy, J.R.; Lee, E.; Gutierrez, A.; He, M.; Park, J.S.; Yonemoto, B.T.; Long, B.R.; Blauwkamp, J.D.; Johnson, C.S.; et al. The Quest for Manganese-Rich Electrodes for Lithium Batteries: Strategic Design and Electrochemical Behavior. *Sustain. Energy Fuels* **2018**, *2*, 1375–1397. [[CrossRef](#)]
36. Chakraborty, A.; Kunnikuruvan, S.; Kumar, S.; Markovsky, B.; Aurbach, D.; Dixit, M.; Major, D.T. Layered Cathode Materials for Lithium-Ion Batteries: Review of Computational Studies on  $\text{LiNi}_{1-x-y}\text{Co}_x\text{Mn}_y\text{O}_2$  and  $\text{LiNi}_{1-x-y}\text{Co}_x\text{Al}_y\text{O}_2$ . *Chem. Mater.* **2020**, *32*, 915–952. [[CrossRef](#)]
37. Yang, P.; Li, H.; Wei, X.; Zhang, S.; Xing, Y. Structure Tuned  $\text{Li}_{1.2}\text{Mn}_{0.6}\text{Ni}_{0.2}\text{O}_2$  with Low Cation Mixing and Ni Segregation as High Performance Cathode Materials for Li-Ion Batteries. *Electrochim. Acta* **2018**, *271*, 276–283. [[CrossRef](#)]
38. Zhu, Y.; Zhang, N.; Zhao, L.; Xu, J.; Liu, Z.; Liu, Y.; Wu, J.; Ding, F. Improving Electrochemical Performance of Lithium-Rich Cathode Material  $\text{Li}_{1.2}\text{Mn}_{0.52}\text{Ni}_{0.13}\text{Co}_{0.13}\text{W}_{0.02}\text{O}_2$  Coated with  $\text{Li}_2\text{WO}_4$  for Lithium Ion Batteries. *J. Alloys Compd.* **2019**, *811*, 152023. [[CrossRef](#)]
39. Hua, W.; Zhang, J.; Zheng, Z.; Liu, W.; Peng, X.; Guo, X.D.; Zhong, B.; Wang, Y.J.; Wang, X. Na-Doped Ni-Rich  $\text{LiNi}_{0.5}\text{Co}_{0.2}\text{Mn}_{0.3}\text{O}_2$  Cathode Material with Both High Rate Capability and High Tap Density for Lithium Ion Batteries. *Dalt. Trans.* **2014**, *43*, 14824–14832. [[CrossRef](#)]
40. Xie, Y.; Yin, J.; Chen, X.; Liang, X.; Jin, Y.; Xiang, L. Synergistic Effect of  $\text{Mn}^{3+}$  Formation-Migration and Oxygen Loss on the near Surface and Bulk Structural Changes in Single Crystalline Lithium-Rich Oxides. *ACS Appl. Mater. Interfaces* **2021**, *13*, 3891–3898. [[CrossRef](#)]
41. Jafta, C.J.; Raju, K.; Mathe, M.K.; Manyala, N.; Ozoemena, K.I. Microwave Irradiation Controls the Manganese Oxidation States of Nanostructured  $(\text{Li}[\text{Li}_{0.2}\text{Mn}_{0.52}\text{Ni}_{0.13}\text{Co}_{0.13}\text{Al}_{0.02}]\text{O}_2)$  Layered Cathode Materials for High-Performance Lithium Ion Batteries. *J. Electrochem. Soc.* **2015**, *162*, A768–A773. [[CrossRef](#)]
42. Jafta, C.J.; Mathe, M.K.; Manyala, N.; Roos, W.D.; Ozoemena, K.I. The Effect of Microwave Treatment on the  $\text{Mn}^{3+}$  Concentration of Spinel Cathode Material Studied By XPS, XRD and Electrochemical Method. In Proceedings of the 224th ECS Meeting, San Francisco, CA, USA, 27 October–1 November 2013; pp. 4–10.
43. Susai, F.A.; Talianker, M.; Liu, J.; Rosy, Paul, T.; Grinblat, Y.; Erickson, E.; Noked, M.; Burstein, L.; Frenkel, A.I.; et al. Electrochemical Activation of  $\text{Li}_2\text{MnO}_3$  Electrodes at 0 °C and Its Impact on the Subsequent Performance at Higher Temperatures. *Materials* **2020**, *13*, 4388. [[CrossRef](#)] [[PubMed](#)]
44. Luo, D.; Ding, X.; Fan, J.; Zhang, Z.; Liu, P.; Yang, X.; Guo, J.; Sun, S.; Lin, Z. Accurate Control of Initial Coulombic Efficiency for Lithium-Rich Manganese-Based Layered Oxides by Surface Multicomponent Integration. *Angew. Chem.—Int. Ed.* **2020**, *59*, 23061–23066. [[CrossRef](#)] [[PubMed](#)]
45. Zuo, Y.; Ma, J.; Jiang, N.; Xia, D. Effects of Particle Size on Voltage Fade for Li-Rich Mn-Based Layered Oxides. *ACS Omega* **2018**, *3*, 11136–11143. [[CrossRef](#)] [[PubMed](#)]
46. Kaewmala, S.; Limphirat, W.; Yordsri, V.; Nash, J.; Srilomsak, S.; Kesorn, A.; Limthongkul, P.; Meethong, N. Rate Dependent Structural Changes, Cycling Stability, and Li-Ion Diffusivity in a Layered–Layered Oxide Cathode Material after Prolonged Cycling. *J. Mater. Chem. A* **2021**, *9*, 14004–14012. [[CrossRef](#)]
47. Jossen, A. Encyclopedia of Electrochemical Power Sources. *Batter. Dyn.* **2009**, *2*, 478–488. [[CrossRef](#)]

48. Song, J.H.; Yoon, G.; Kim, B.; Eum, D.; Park, H.; Kim, D.H.; Kang, K. Anionic Redox Activity Regulated by Transition Metal in Lithium-Rich Layered Oxides. *Adv. Energy Mater.* **2020**, *10*, 2001207. [[CrossRef](#)]
49. Aang, Y.; Shang, K.; He, W.; Ai, X.; Cao, Y.; Yang, H. Magnesium-Doped  $\text{Li}_{1.2}[\text{Co}_{0.13}\text{Ni}_{0.13}\text{Mn}_{0.54}]\text{O}_2$  for Lithium-Ion Battery Cathode with Enhanced Cycling Stability and Rate Capability. *ACS Appl. Mater. Interfaces* **2015**, *7*, 13014–13021. [[CrossRef](#)]
50. Wang, E.; Zhao, Y.; Xiao, D.; Zhang, X.; Wu, T.; Wang, B.; Zubair, M.; Li, Y.; Sun, X.; Yu, H. Composite Nanostructure Construction on the Grain Surface of Li-Rich Layered Oxides. *Adv. Mater.* **2020**, *32*, 1906070. [[CrossRef](#)]
51. Zhang, X.D.; Shi, J.L.; Liang, J.Y.; Yin, Y.X.; Zhang, J.N.; Yu, X.Q.; Guo, Y.G. Suppressing Surface Lattice Oxygen Release of Li-Rich Cathode Materials via Heterostructured Spinel  $\text{Li}_4\text{Mn}_5\text{O}_{12}$  Coating. *Adv. Mater.* **2018**, *30*, 1801751. [[CrossRef](#)]
52. Wang, N.; Chen, Y.; Yin, J.; Yan, W.; Li, F.; Jin, Y. Systematic Study of the Effects of Lithium Deficiencies on the Crystal Structure and Electrochemical Performance of Li-Rich Materials. *J. Alloys Compd.* **2022**, *900*, 163549. [[CrossRef](#)]
53. Zhang, K.; Li, B.; Zuo, Y.; Song, J.; Shang, H.; Ning, F.; Xia, D. Voltage Decay in Layered Li-Rich Mn-Based Cathode Materials. *Electrochem. Energy Rev.* **2019**, *2*, 606–623. [[CrossRef](#)]
54. Yan, P.; Nie, A.; Zheng, J.; Zhou, Y.; Lu, D.; Zhang, X.; Xu, R.; Belharouak, I.; Zu, X.; Xiao, J.; et al. Evolution of Lattice Structure and Chemical Composition of the Surface Reconstructions Layer in  $\text{Li}_{1.2}\text{Ni}_{0.2}\text{Mn}_{0.6}\text{O}_2$  Cathode Material for Lithium Ion Batteries. *Nano Lett.* **2015**, *15*, 514–522. [[CrossRef](#)]
55. Hua, W.; Wang, S.; Knapp, M.; Leake, S.J.; Senyshyn, A.; Richter, C.; Yavuz, M.; Binder, J.R.; Grey, C.P.; Ehrenberg, H.; et al. Structural Insights into the Formation and Voltage Degradation of Lithium- and Manganese-Rich Layered Oxides. *Nat. Commun.* **2019**, *10*, 5365. [[CrossRef](#)]
56. Fang, L.; Zhou, L.; Park, M.; Han, D.; Lee, G.-H.; Kang, S.; Lee, S.; Chen, M.; Hu, Z.; Zhang, K.; et al. Hysteresis Induced by Incomplete Cationic Redox in Li-Rich 3d-Transition-Metal Layered Oxides Cathodes. *Adv. Sci.* **2022**, *9*, 220196. [[CrossRef](#)]
57. Zhang, Y.; Zhang, W.; Shen, S.; Yan, X.; Wu, R.; Wu, A.; Lastoskie, C.; Zhang, J. Sacrificial Template Strategy toward a Hollow  $\text{LiNi}_{1/3}\text{Co}_{1/3}\text{Mn}_{1/3}\text{O}_2$  Nanosphere Cathode for Advanced Lithium-Ion Batteries. *ACS Omega* **2017**, *2*, 7593–7599. [[CrossRef](#)]
58. Xu, Y.; Zhang, M.; Yi, L.; Liang, K.  $\text{Fe}^{3+}$  and  $\text{PO}_4^{3-}$  Co-Doped Li-Rich  $\text{Li}_{1.20}\text{Mn}_{0.56}\text{Ni}_{0.16}\text{Co}_{0.08}\text{O}_2$  as Cathode with Outstanding Structural Stability for Lithium-Ion Battery. *J. Alloys Compd.* **2021**, *865*, 158899. [[CrossRef](#)]
59. An, J.; Shi, L.; Chen, G.; Li, M.; Liu, H.; Yuan, S.; Chen, S.; Zhang, D. Insights into the Stable Layered Structure of a Li-Rich Cathode Material for Lithium-Ion Batteries. *J. Mater. Chem. A* **2017**, *5*, 19738–19744. [[CrossRef](#)]
60. Liang, Y.; Li, S.; Xie, J.; Yang, L.; Li, W.; Li, C.; Ai, L.; Fu, X.; Cui, X.; Shangguan, X. Synthesis and Electrochemical Characterization of Mg-Al Co-Doped Li-Rich Mn-Based Cathode Materials. *New J. Chem.* **2019**, *43*, 12004–12012. [[CrossRef](#)]
61. Shanmugam, V.; Natarajan, S.; Lobo, L.S.; Mathur, A.; Sahana, M.B.; Sundararajan, G.; Gopalan, R. Surface Oxygen Vacancy Engineering and Physical Protection by In-Situ Carbon Coating Process of Lithium Rich Layered Oxide. *J. Power Sources* **2021**, *515*, 230623. [[CrossRef](#)]
62. Zhang, X.; Hao, J.; Wu, L.; Guo, Z.; Ji, Z.; Luo, J.; Chen, C.; Shu, J.; Long, H.; Yang, F.; et al. Enhanced Electrochemical Performance of Perovskite  $\text{LaNiO}_3$  Coating on  $\text{Li}_{1.2}\text{Mn}_{0.54}\text{Ni}_{0.13}\text{Co}_{0.13}\text{O}_2$  as Cathode Materials for Li-Ion Batteries. *Electrochim. Acta* **2018**, *283*, 1203–1212. [[CrossRef](#)]
63. Chen, W.C.; Song, Y.F.; Wang, C.C.; Liu, Y.; Morris, D.T.; Pianetta, P.A.; Andrews, J.C.; Wu, H.C.; Wu, N.L. Study on the Synthesis-Microstructure-Performance Relationship of Layered Li-Excess Nickel-Manganese Oxide as a Li-Ion Battery Cathode Prepared by High-Temperature Calcination. *J. Mater. Chem. A* **2013**, *1*, 10847–10856. [[CrossRef](#)]
64. Wang, M.-J.; Yu, F.-D.; Sun, G.; Gu, D.-M.; Wang, Z.-B. Optimizing the Structural Evolution of Li-Rich Oxide Cathode Materials via Microwave-Assisted Pre-Activation. *ACS Appl. Energy Mater.* **2018**, *1*, 4158–4168. [[CrossRef](#)]
65. Bao, Y.; Wang, J.; Qian, Y.; Deng, Y.; Yang, X.; Chen, G. An Appropriate Amount of New Spinel Phase Induced by Control Synthesis for the Improvement of Electrochemical Performance of Li-Rich Layered Oxide Cathode Material. *Electrochim. Acta* **2020**, *330*, 135240. [[CrossRef](#)]

**Disclaimer/Publisher's Note:** The statements, opinions and data contained in all publications are solely those of the individual author(s) and contributor(s) and not of MDPI and/or the editor(s). MDPI and/or the editor(s) disclaim responsibility for any injury to people or property resulting from any ideas, methods, instructions or products referred to in the content.